Available online at www.sciencedirect.com
SCIENCE DIRECT®
Advances in Water Resources 28 (2005) 661–670
Advances in Water Resources
www.elsevier.com/locate/advwatres

Kinematic wave modeling of overland flow using characteristics method with cubic-spline interpolation

Tung-Lin Tsai [a,*], Jinn-Chuang Yang [b]

[a] Natural Hazard Mitigation Research Center, National Chiao Tung University, 1001 Ta Hsueh Road, Hsinchu 30010, Taiwan, ROC
[b] Department of Civil Engineering, National Chiao Tung University, Hsinchu 30010, Taiwan, ROC

Received 11 March 2004; received in revised form 14 December 2004; accepted 24 January 2005
Available online 11 March 2005

Abstract

Use of characteristics method integrated with cubic-spline interpolation technique (CSMOC scheme) for computation of one-dimensional and two-dimensional kinematic overland flow has been examined in this study. The characteristic trajectory is allowed to fall on space line and time line for interpolating the corresponding values at the foot of trajectory in terms of neighboring grid points. The effects of different endpoint constraints on use of cubic-spline interpolation are investigated. As far as accuracy and simplicity are concerned, the not-a-knot constraint could be a better choice. Three hypothetical examples are used to examine the capabilities of CSMOC scheme through the comparison with the analytical solution and the well-known Preissmann scheme. Some degrees of numerical diffusion and numerical oscillation, attenuating and overestimating the peak discharge, are induced by the Preissmann scheme. In contrast, the CSMOC scheme gives convincing results for the kinematic overland flow computations.

Keywords: Overland flow; Kinematic wave; Characteristics method; Runoff; Cubic-spline interpolation; Hydrology

1. Introduction

The kinematic wave equation approximation to the Saint-Venant hydrodynamic equations is frequently applied to the overland flow computations due to its simplicity. The kinematic wave theory is also often sufficiently accurate for flow modeling, where the backwater effects and the flow acceleration are not important. Growing environmental and ecological concerns have increased the role of the kinematic wave theory in modeling hydraulic processes [20]. Hjelmfelt [9], Parlange et al. [19], Govindaraju et al. [6,7], and Singh [20] have generated analytical or semianalytical solutions for the kinematic wave equations with simplified conditions. However, for most realistic problems in which rainfall, infiltration and surface characteristics vary randomly in space and time, the analytical solutions for the kinematic wave equations are not tractable and the numerical approach is the only choice.

The finite difference method and the finite element method are two common numerical approaches used for the kinematic overland flow computations. For example, de Lima and Singh [4] used the Lax–Wendroff scheme to investigate the influence of the pattern of moving rainstorms on overland flow. Holden and Stephenson [10] applied the Preissmann scheme for the overland flow computation and assessed the effects of grid space and the spatial and temporal weighting coefficients on it. In addition, numerous studies on solving the kinematic wave problems using the Galerkin finite element scheme have been reported [8,21,11]. However,

* Corresponding author. Tel.: +886 3 5131468; fax: +886 3 5734116.
E-mail addresses: tltsai@mail.nctu.edu.tw (T.-L. Tsai), jcyang@mail.nctu.edu.tw (J.-C. Yang).

0309-1708/$ - see front matter © 2005 Elsevier Ltd. All rights reserved.
doi:10.1016/j.advwatres.2005.01.005

Nomenclature

h	water depth	θ	time position weight
q	flow rate per unit width	Δx	computational grid interval
r	excessive rainfall rate	Δt	time increment
A–D	coefficients of the cubic-spline interpolation		
N	Manning roughness coefficient	*Subscript*	
S	second derivative	i	x-directional computational point index
S_0	bottom slope		
S_f	friction slope	*Superscript*	
ϕ	longitudinal space weight	n	time step index

use of the finite difference method and the finite element method could induce some degree of numerical diffusion or numerical oscillation that can attenuate or overestimate the peak discharge of flow.

The method of characteristics is known to have many advantages for the theoretical and physical interpretation of flow patterns. The method of characteristics can be classified into two categories, i.e., the characteristics-grid scheme and the specified-time-interval scheme. The specified-time-interval scheme is the popular scheme for hydraulic engineering problems because of its practicability. With the specified-time-interval scheme, the characteristic trajectory usually does not pass through the grid points. An interpolation technique is needed to obtain corresponding values at the foot of the trajectory. Thus, the accuracy of characteristics method is strongly related to the form of interpolation technique.

Use of the characteristics method with linear interpolation leads to an inevitable smoothing of the solution for flow modeling [16–18,28]. In order to efficiently reduce the numerical errors induced by linear interpolation, the cubic-spline interpolation, a kind of piecewise cubic approximation, was first applied by Schohl and Holly [22] in one-dimensional advective solute transport and then applied to the two-dimensional advection–diffusion equation by Karpik and Crockett [13] and Stefanovic and Stefan [23]. The cubic-spline interpolation originally developed on the space line had also been extended to the time line [1], which allows the characteristic curve to fall on the temporal axis. Tsai et al. [27] investigated the effects of different kinds of endpoint constraints on the use of cubic-spline interpolation for solving the advection–diffusion equation.

The goal of this paper is to examine the applicability of the characteristics method integrated with cubic-spline interpolation technique for one-dimensional and two-dimensional kinematic overland flow computations. In this study, the method of characteristics integrated with cubic-spline interpolation technique is called CSMOC scheme. In the following sections, the mathematical and numerical formulations for the CSMOC scheme in modeling the kinematic overland flow are first introduced. The effects of endpoint constraints on use of cubic-spline interpolation are then examined. Finally, the comparison study for the results from the CSMOC scheme, the analytical solutions, and the well-known Preissmann scheme are conducted on some one-dimensional and two-dimensional hypothetical examples.

2. Governing equations

Any appropriate mathematical formulation of the overland flow makes use of the fundamental mass and momentum equations. The equation of continuity for shallow water flow, representing the conservation of mass, can be written in one dimension as

$$\frac{\partial h}{\partial t}+\frac{\partial q}{\partial x}=r(x,t) \tag{1}$$

where q = flow rate per unit width; h = flow depth; x = distance in the flow direction; t = time; r = excess rainfall rate.

A flow-resistance equation, derived by neglecting the inertia force and the pressure force in the momentum equation ($S_0 = S_f$), can be represented as

$$q=\alpha h^{\beta} \tag{2}$$

where, using Manning's equation, $\alpha = S_0^{1/2}/N$; $\beta = 5/3$ in which N is the Manning's roughness coefficient; S_0 and S_f are the bottom slope and the friction slope, respectively.

Substituting Eq. (2) into Eq. (1), the kinematic wave equation for the overland flow can be represented as

$$\frac{\partial h}{\partial t}+\alpha\beta h^{\beta-1}\frac{\partial h}{\partial x}=r(x,t) \tag{3}$$

Eq. (3) can be rewritten as

$$\frac{Dh}{Dt}=r(x,t) \tag{4}$$

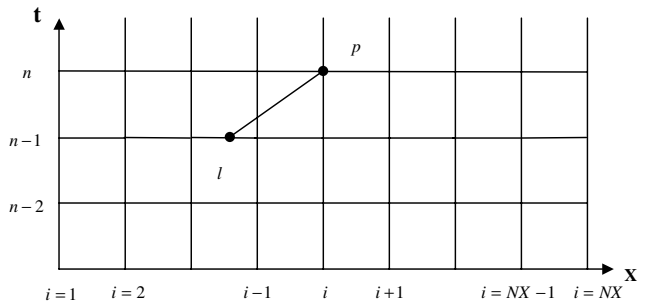

Fig. 1. Grid system of characteristics method with cubic-spline interpolation.

along with

$$\frac{dx}{dt} = \alpha\beta h^{\beta-1} \tag{5}$$

where $D/D_t = (\partial/\partial t) + (dx/dt)(\partial/\partial x)$ denotes the total derivative. Eq. (5) represents the characteristic curve shown in Fig. 1.

3. Numerical framework of characteristics method with cubic-spline interpolation

By integrating Eqs. (4) and (5) along the characteristic curve from l to p shown in Fig. 1 and applying the trapezoidal-rule approximation to the time integration term yields

$$h_p - h_l = \frac{\Delta t}{2}(r_p + r_l) \tag{6}$$

and

$$x_p - x_l = \frac{\alpha\beta\Delta t}{2}\left(h_p^{\beta-1} + h_l^{\beta-1}\right) \tag{7}$$

The points l and p are two nodal points of the characteristic trajectory. h_p is the unknown water depth of grid point p at time level n, which is to be solved. h_l is water depth of point l at time level $n-1$, in which water depths of all grid points are known. The nodal point l does not usually coincide with any grid point. Several forms of interpolation techniques could be used to approximate h_l. The cubic-spline interpolation is to construct a piecewise cubic polynomial function of the dependent variable between two grid points such that the interpolating function must pass through each node and be continuous in its first and second derivatives at interior nodes.

When the characteristic curve intersects the space line at time level $n-1$, shown in Fig. 1, the cubic-spline interpolation can be used to evaluate h_l corresponding to all known grid values of h at time level $n-1$, i.e., h_i^{n-1}, $i = 1,2,\ldots,NX$. From the description of the cubic-spline interpolation mentioned above, the second derivative of h at time level $n-1$ is a continuous piecewise linear function between each two grid points, that is

$$h^{n-1}(x)'' = S_i\frac{x_{i+1}-x}{\Delta x} + S_{i+1}\frac{x-x_i}{\Delta x} \quad x \in [x_i, x_{i+1}] \tag{8}$$

where $i = 1,2,\ldots,NX-1$ in the uniform grid space $\Delta x = x_{i+1} - x_i$. $h^{n-1}(x)''$ is the function of second derivative of h at time level $n-1$. S_i and S_{i+1} denote the second derivative of h at time level $n-1$ and grid points i and $i+1$, respectively. Integrating Eq. (8) twice with respect to x and substituting the nodal values at grid points i and $i+1$ yields the expression for the cubic function $h^{n-1}(x)$ on interval x_i to x_{i+1}

$$\begin{aligned} h^{n-1}(x) = {} & S_i\frac{(x_{i+1}-x)^3}{6\Delta x} + S_{i+1}\frac{(x-x_i)^3}{6\Delta x} \\ & + \left(h_i^{n-1} - S_i\frac{\Delta x^2}{6}\right)\frac{x_{i+1}-x}{\Delta x} \\ & + \left(h_{i+1}^{n-1} - S_{i+1}\frac{\Delta x^2}{6}\right)\frac{x-x_i}{\Delta x} \end{aligned} \tag{9}$$

The second derivative with respect to space at grid points shown in Eq. (9) can be obtained by using the continuity of the first derivative with respect to space at interior nodes

$$\begin{aligned} & S_{i-1} + 2S_i + S_{i+1} = \frac{6}{\Delta x^2}\left(h_{i+1}^{n-1} - 2h_i^{n-1} + h_{i-1}^{n-1}\right) \\ & i = 2,\ldots,NX-1 \end{aligned} \tag{10}$$

The system of equations in Eq. (10) is underdetermined since it involves only $NX-2$ equations for finding NX unknowns. Two additional constraints at endpoints, i.e., S_1 and S_{NX}, must be added to close this system. Four types of endpoint constraints [5,14,15,27] may be used to produce the various types of cubic-spline interpolations. They are stated below:

1. First derivative endpoint constraints:

$$2\Delta x S_1 + \Delta x S_2 = 6\left(\frac{h_2^{n-1} - h_1^{n-1}}{\Delta x} - \frac{\partial h(x_1)}{\partial x}\right) \tag{11a}$$

and

$$2\Delta x S_{NX} + \Delta x S_{NX-1} = 6\left(\frac{\partial h(x_{NX})}{\partial x} - \frac{h_{NX}^{n-1} - h_{NX-1}^{n-1}}{\Delta x}\right) \tag{11b}$$

2. Second derivative endpoint constraints:

$$S_1 = \frac{\partial^2 h(x_1)}{\partial x^2} \tag{12a}$$

and

$$S_{NX} = \frac{\partial^2 h(x_{NX})}{\partial x^2} \tag{12b}$$

3. Quadratic endpoint constraints:

$$S_1 = S_2 \tag{13a}$$

and

$$S_{NX} = S_{NX-1} \tag{13b}$$

4. Not-a-knot endpoint constraints:

$$S_1 = 2S_2 - S_3 \tag{14a}$$

and

$$S_{NX} = 2S_{NX-1} - S_{NX-2} \tag{14b}$$

In Eqs. (11) and (12), the unknown first and second derivatives could be obtained by finite difference approximation corresponding to grid points near the boundary. However, the frequently used natural cubic-spline interpolation simply takes $S_1 = S_{NX} = 0$ in Eq. (12) and neglects the second derivative at endpoints. Thus, it makes the end cubics approach linearity at their extremities. On the other hand, by substituting Eq. (13) into Eq. (9), one can clearly find that this endpoint constraint is equivalent to assuming that the end cubics approach to quadratic curves at their extremities. The not-a-knot endpoint constraint shown in Eq. (14) represents the continuity of the third derivative at the nodes x_2 and x_{NX-1} [3]. In other words, two cubic segments that join at the node x_2 are adjacent parts of the same cubic curve. The identical result as that at node x_2 is also yielded at node x_{NX-1}.

The system of equations shown in Eq. (10) associated with additional endpoint constraints shown in Eqs. (11)–(14) can be easily and efficiently solved by the Thomas algorithm [24].

According to cubic-spline interpolation given by Eq. (9) and the distance between x_p and x_l shown in Eq. (7), h_l can be evaluated as

$$h_l = A_{i-\hat{n}_l-1}[(1-\omega)\Delta x]^3 + B_{i-\hat{n}_l-1}[(1-\omega)\Delta x]^2 + C_{i-\hat{n}_l-1}[(1-\omega)\Delta x] + D_{i-\hat{n}_l-1} \tag{15}$$

with

$$\omega = \frac{(h)_{pl}\Delta t}{\Delta x} - \hat{n}_l \tag{16}$$

where $(h)_{pl} = \alpha\beta(h_p^{\beta-1} + h_l^{\beta-1})/2$; $\hat{n}_l = \mathrm{INT}[(h)_{pl}\Delta t/\Delta x]$ in which INT denotes the integral portion. The coefficients A_j, B_j, C_j, and D_j shown in Eq. (15) can be written as

$$A_j = \frac{S_{j+1} - S_j}{6\Delta x} \tag{17}$$

$$B_j = \frac{S_j}{2} \tag{18}$$

$$C_j = \frac{h_{j+1}^{n-1} - h_j^{n-1}}{\Delta x} - \frac{2\Delta x S_j + \Delta x S_{j+1}}{6} \tag{19}$$

$$D_j = h_j^{n-1} \tag{20}$$

where $j = 1, 2, \ldots, NX-1$. With known h_l, h_p is then obtained from Eq. (6). An iterative solution procedure shown in Fig. 2 is needed to complete above computation as follows:

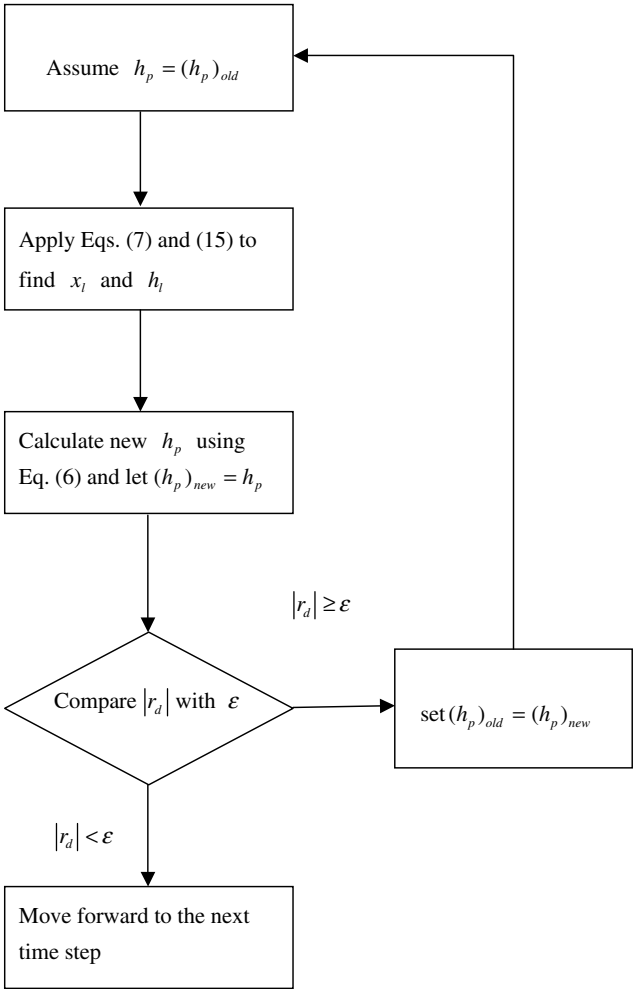

Fig. 2. Flow chart of the characteristics method with cubic-spline interpolation for computation of kinematic overland flow.

1. Give an assumed value of water depth at grid i and time level n, i.e. $h_p = (h_p)_{\mathrm{old}}$.
2. Apply Eqs. (7) and (15) to find x_l and h_l with the given water depth in step 1.
3. Calculate new h_p using Eq. (6) with known h_l found from step 2, and then let $(h_p)_{\mathrm{new}} = h_p$.
4. Compare the relative difference $r_{\mathrm{d}} = \lfloor (h_p)_{\mathrm{new}} - (h_p)_{\mathrm{old}} \rfloor / (h_p)_{\mathrm{old}}$ with the tolerant error ε ($\varepsilon = 0.001$ is used in this study).
5. If $|r_{\mathrm{d}}|$ is less than ε, the computation moves forward to the next time step.
6. If $|r_{\mathrm{d}}|$ is larger than or equals ε, set $(h_p)_{\mathrm{old}} = (h_p)_{\mathrm{new}}$ and repeat step 1 to step 6.

In the solution procedure mentioned above, the characteristic curve will intersect the time line at boundary shown in Fig. 3 when the ratio of Δt to Δx is too large, i.e. $(h)_{pl}\Delta t/\Delta x \geqslant i - 1$. The cubic-spline interpolation

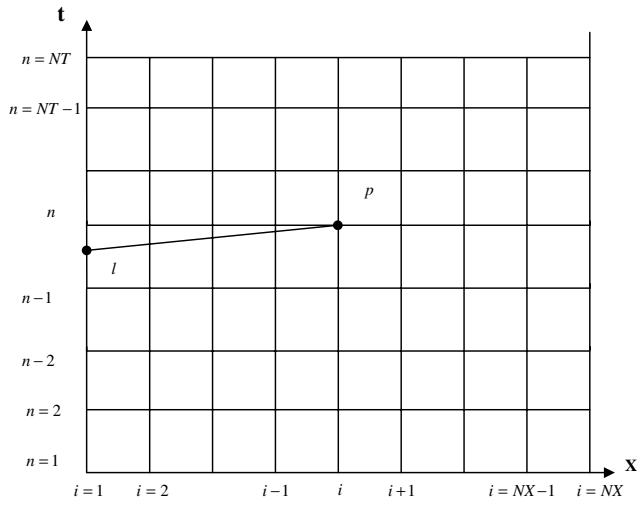

Fig. 3. Grid system of characteristics method with cubic-spline interpolation at boundary.

technique can also be applied to the time line to approximate h_l shown in Appendix A.

4. Extension to two-dimensional problems

The above derivation for solving one-dimensional kinematic overland flow problems can be extended by the method of fractional steps [25,26,30] to two-dimensional cases without difficulty. The governing equation for the two-dimensional kinematic overland flow can be represented as

$$\frac{\partial h}{\partial t} + \alpha_x \beta h^{\beta-1} \frac{\partial h}{\partial x} + \alpha_y \beta h^{\beta-1} \frac{\partial h}{\partial y} = r(x, y, t) \tag{21}$$

where, using Manning's equation, $\alpha_x = S_{0x}^{1/2}/N$ and $\alpha_y = S_{0y}^{1/2}/N$ in which N is the Manning's roughness coefficient; S_{0x} and S_{0y} are the bed slopes in the x and y directions, respectively. Using the method of fractional steps, Eq. (21) can be approximated with a series of one-dimensional kinematic overland flow equations as

$$\frac{\partial h}{\partial t} + \alpha_x \beta h^{\beta-1} \frac{\partial h}{\partial x} = \frac{r(x, y, t)}{2} \tag{22}$$

and

$$\frac{\partial h}{\partial t} + \alpha_y \beta h^{\beta-1} \frac{\partial h}{\partial y} = \frac{r(x, y, t)}{2} \tag{23}$$

Eqs. (22) and (23) can each be solved by the characteristics method integrated with the cubic-spline interpolation on the basis of one dimension shown in Eqs. (6), (7) and (15).

5. Examination of endpoint constraints

In this section, a sloping plane with length of 900 m and slope of 0.02 subject to a steady uniform rainfall rate $r = 30$ cm/h with duration of 3000 s is applied to examine the effects of different endpoint constraints on use of the cubic-spline interpolation for solving the kinematic overland flow. The initial and the upstream boundary conditions, respectively, are taken as $q = h = 0$ at $t = 0$ for all x; and $q = h = 0$ at $x = 0$ for all t. The grid space $\Delta x = 100$ m, 150 m, and 180 m are respectively used in this simulation. Tables 1 and 2 display the simulated results from different endpoint constraints in terms of peak discharge and root mean square error of discharge at $x = 900$ m with time step $\Delta t = 80$ s, and Manning's roughness coefficient $N = 0.02$. One can observe from Tables 1 and 2 that the more accurate simulated results are obtained by use of small grid space. The natural constraint and the first derivative constraint with first-order finite difference approximation induce large numerical diffusion and have worse simulated results than the other constraints. This is due to the fact that these two constraints approach the end cubics to linear ones at their extremities. The not-a-knot constraint produces better simulated results than the quadratic constraint. The computational results of the first and second derivative constraints are related to the derivative approximations, especially for the use of lower-order finite difference approximation. The better simulated results, competitive to those from the not-a-knot constraint, are obtained by the application of higher-order finite difference approximation to the first and second constraints. Thus, as far as the accuracy and simplicity are concerned, the not-a-knot constraint seems to be a better choice. In the following section, only the not-a-knot constraint is employed in the CSMOC scheme.

6. Demonstration and evaluation

6.1. One-dimensional examples

Two hypothetical examples are used to examine the CSMOC scheme for solving the one-dimensional kinematic overland flow as compared with the well-known Preissmann scheme. The Preissmann formulation of the continuity equation for the overland flow shown in (1) can be expressed as

$$\frac{\theta\left(h_{i-1}^{n} - h_{i-1}^{n-1}\right) + (1-\theta)\left(h_{i}^{n} - h_{i}^{n-1}\right)}{\Delta t} + \frac{\phi\left(q_{i}^{n-1} - q_{i-1}^{n-1}\right) + (1-\phi)\left(q_{i}^{n} - q_{i-1}^{n}\right)}{\Delta x} = r \tag{24}$$

where ϕ and θ are a time position weight and a longitudinal space weight, respectively. $\phi = 0$, $\phi = 0.5$, and $\phi = 1$ respectively result in explicit, centred, and implicit schemes. Brakensiek [2] showed that the latter two schemes were more stable than the explicit one. Holden

Table 1
Peak discharge (m^2/s) at $x = 900$ m for various endpoint constraints (the exact peak discharge is 0.075 m^2/s)

Constraints	Grid size		
	$\Delta x = 100$ m	$\Delta x = 150$ m	$\Delta x = 180$ m
Natural	0.0734	0.0722	0.0715
Quadratic	0.0747	0.0736	0.0730
Not-a-knot	0.0750	0.0749	0.0748
First derivative			
1st Order	0.0733	0.0720	0.0713
2nd Order	0.0742	0.0735	0.0729
3rd Order	0.0750	0.0748	0.0746
4th Order	0.0750	0.0750	0.0748
5th Order	0.0750	0.0749	0.0749
Second derivative			
1st Order	0.0737	0.0726	0.0720
2nd Order	0.0746	0.0743	0.0740
3rd Order	0.0750	0.0749	0.0747
4th Order	0.0750	0.0750	0.0749

Table 2
Root mean square error of discharge (m^2/s) at $x = 900$ m for various endpoint constraints

Constraints	Grid size		
	$\Delta x = 100$ m	$\Delta x = 150$ m	$\Delta x = 180$ m
Natural	0.000879 (1.17%)[a]	0.00155 (2.06%)	0.00195 (2.60%)
Quadratic	0.000761 (1.01%)	0.00134 (1.78%)	0.00169 (2.25%)
Not-a-knot	0.000640 (0.85%)	0.00101 (1.34%)	0.00133 (1.77%)
First derivative			
1st Order	0.000953 (1.27%)	0.00167 (2.22%)	0.00211 (2.81%)
2nd Order	0.000761 (1.01%)	0.00139 (1.85%)	0.00175 (2.33%)
3rd Order	0.000645 (0.86%)	0.00104 (1.38%)	0.00136 (1.81%)
4th Order	0.000639 (0.85%)	0.00100 (1.33%)	0.00133 (1.77%)
5th Order	0.000644 (0.86%)	0.00103 (1.37%)	0.00133 (1.77%)
Second derivative			
1st Order	0.000799 (1.06%)	0.00137 (1.82%)	0.00173 (2.31%)
2nd Order	0.000646 (0.86%)	0.00107 (1.42%)	0.00136 (1.81%)
3rd Order	0.000638 (0.85%)	0.00103 (1.37%)	0.00132 (1.76%)
4th Order	0.000641 (0.85%)	0.00102 (1.36%)	0.00129 (1.72%)

[a] The percentage represents the ratio between the exact peak discharge (0.075 m^2/s) at $x = 900$ m and the root mean square error of computed discharge from various endpoint constraints.

and Stephenson [10] further pointed out that a central-difference formulation should be used to prevent numerical diffusion for solving the kinematic wave equations. In addition, Weinmann and Laurenson [29] showed that θ must lie between 0 and 0.5 for a valid solution when the temporal derivative is centred, i.e. $\phi = 0.5$. Thus, in this study, the Preissmann scheme with $\phi = 0.5$, $\theta = 0$ and $\phi = 0.5$, $\theta = 0.5$ are respectively used for the kinematic overland flow computations.

The first example is the overland flow on a sloping plane with length of 1000 m and slope of 0.01 subject to a steady uniform excess rainfall rate $r = 30$ cm/h with duration of 1600 s. The following parameters are used in the numerical simulation: grid space $\Delta x = 50$ m, time step $\Delta t = 80$ s, and Manning's roughness coefficient $N = 0.02$. The initial and the upstream boundary condi-

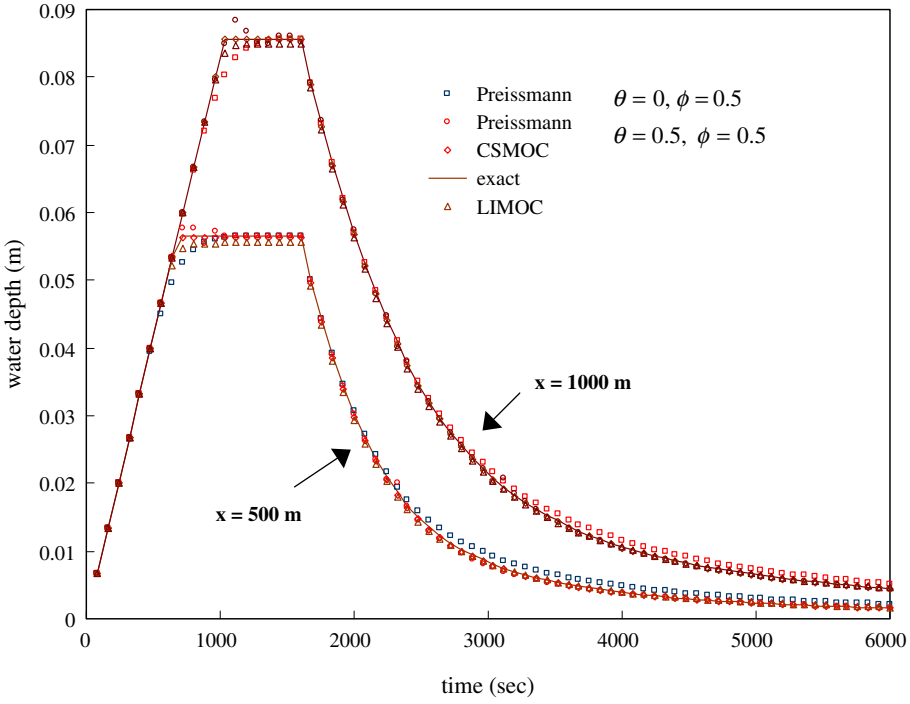

Fig. 4. The simulated results of water depth at 500 m and 1000 m downstream from the upstream boundary for the case of steady excess rainfall rate.

tions, respectively, are taken as $q = h = 0$ at $t = 0$ for all x; and $q = h = 0$ at $x = 0$ for all t. The analytical solution [20] and the simulated results in terms of the water depth with respect to time at position 500 m and 1000 m downstream from the upstream boundary by the CSMOC scheme, the LIMOC scheme (the characteristics method with linear interpolation), and the Preissmann scheme are shown in Fig. 4. One can clearly see that the simulated results by the CSMOC scheme almost agree with the analytical solutions, whereas the computational results by the Preissmann scheme and the LIMOC scheme have some deviations from the exact solutions. The Preissmann scheme with $\phi = 0.5$, $\theta = 0.5$ produces some degree of numerical oscillation, especially for the estimation of water depth at peak discharge of outflow. The Preissmann scheme using $\phi = 0.5$, $\theta = 0$ results in the attenuation of peak discharge of outflow and the overestimation of the discharge in the recession process of overland flow. Thus, for values of θ between 0 and 0.5, various degrees of numerical diffusion or numerical oscillation will be introduced by the Preissmann scheme. The root mean square error (RMSE) of water depth at position 500 m and 1000 m downstream from the upstream boundary by various schemes used for comparison herein is shown in Table 3.

The case of unsteady uniform excess rainfall is employed for the further examination of the kinematic overland flow computation by the use of the CSMOC scheme. The unsteady uniform excess rainfall lasts for 4500 s. The excess rainfall rate is $r = 10$ cm/h from the beginning to 1500 s and from 3000 s to 4500 s. A triple excess rainfall rate happens between 1500 s and 3000 s.

Table 3
Root mean square error of water depth at $x = 500$ m and $x = 1000$ m for various schemes

Schemes	Positions	
	$x = 500$ m	$x = 1000$ m
Preissmann $\theta = 0$, $\phi = 0.5$	0.00100	0.00105
Preissmann $\theta = 0.5$, $\phi = 0.5$	0.00035	0.00047
CSMOC	0.00018	0.00017
LIMOC	0.00059	0.00050

The corresponding surface characteristics of sloping plane, such as slope, length, and Manning's roughness coefficient, are the same as those used in the first example. In addition, the initial and the boundary conditions applied are identical to the first example. With grid space of 100 m and time step of 150 s, the simulated water depth with respect to time at position 1000 m downstream form the upstream boundary by the analytical solution, the Preissmann scheme, the CSMOC scheme, and the LIMOC scheme are shown in Fig. 5. Again a numerical oscillation appears in the Preissmann scheme with $\phi = 0.5$, $\theta = 0.5$, and the numerical dissipation results from the LIMOC scheme and the Preissmann scheme with $\phi = 0.5$, $\theta = 0$. The simulated result from the CSMOC scheme is in good agreement with the analytical solution. The RMSE of water depth at position 1000 m downstream from the upstream boundary by the CSMOC scheme, the LIMOC scheme, and the Preissmann scheme with $\phi = 0.5$, $\theta = 0.5$ and $\phi = 0.5$, $\theta = 0$ are 0.0025, 0.00379, 0.00377 and 0.00384, respectively.

From the simulated results of above two hypothetical examples, one could conclude that the CSMOC scheme

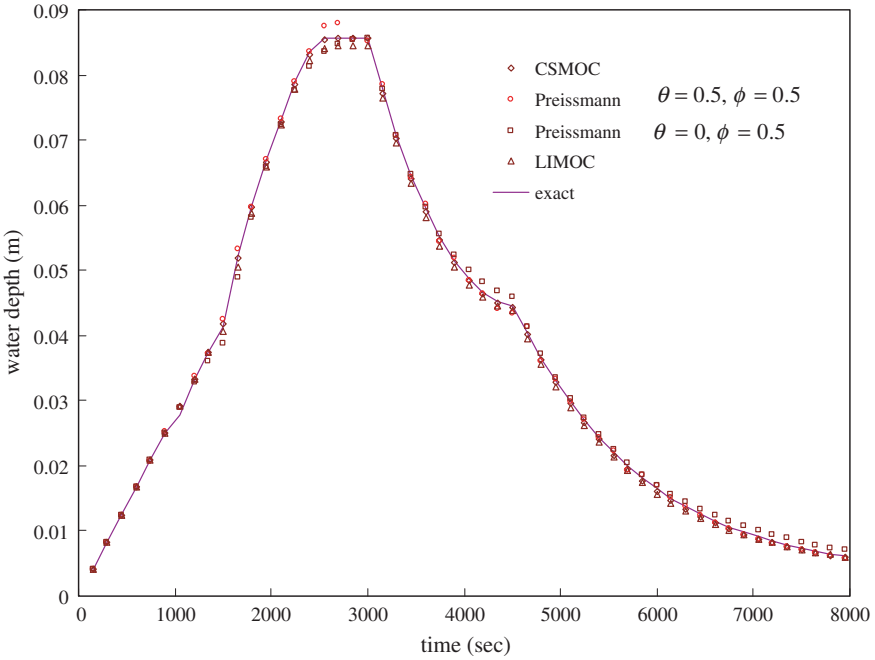

Fig. 5. The simulated results of water depth at 1000 m downstream from the upstream boundary for the case of unsteady excess rainfall rate.

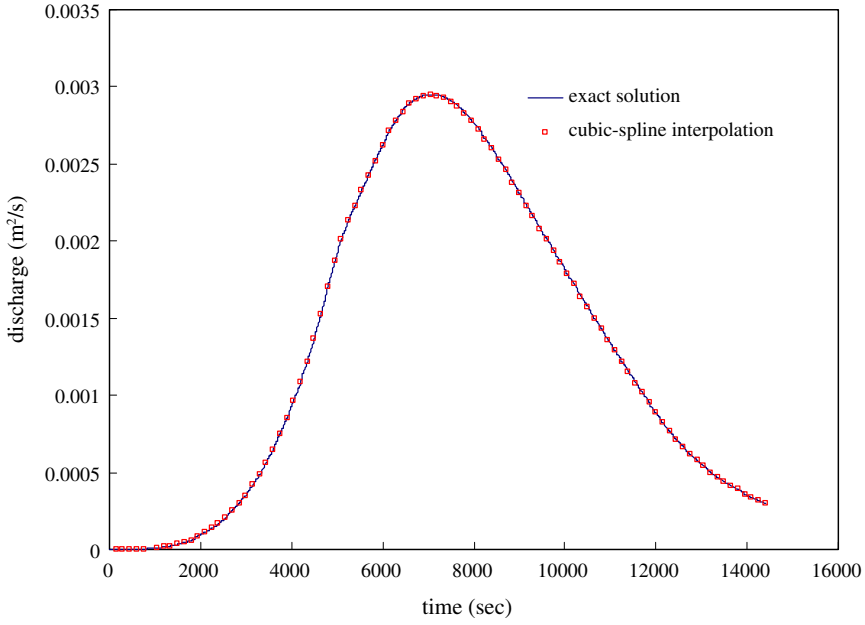

Fig. 6. Hydrograph of discharge of two-dimensional overland flow using characteristics method with cubic-spline interpolation.

can accurately compute the one-dimensional kinematic overland flow and seems to be superior to the LIMOC scheme and the well-known Preissmann scheme.

6.2. Two-dimensional example

A sloping plane of 500 m × 400 m is subject to an unsteady uniform excess rainfall rate with duration of 200 min. The rainfall pattern is given by a triangular hyetograph with a peak rainfall of 2.88 cm/h, i.e., $r(t = 0\ \text{min}) = r(t = 200\ \text{min}) = 0$ cm/h and $r(t = 100\ \text{min}) = 2.88$ cm/h. The slopes of the plane in the x and y directions are

$$S_{0x} = 0.02 + 0.0000149x \tag{25}$$

and

$$S_{0y} = 0.05 + 0.0000116y \tag{26}$$

In addition, Manning's roughness coefficient is

$$N = \sqrt{(0.1 - 0.0000168x)^2 + (0.1 - 0.0000168y)^2} \tag{27}$$

A grid size of 25 m × 25 m and a time step of 80 s are used in the numerical simulation. The initial condition is taken as $q = h = 0$ at $t = 0$ for all x and y. The boundary conditions are $q = h = 0$ at $x = 0$ and $y = 0$ for all t.

The simulated results in terms of discharge with respect to time at the outlet node of coordinates of (500 m, 400 m) by the CSMOC scheme, and the proposed analytical solution are shown in Fig. 6. The proposed analytical solution was obtained by the Galerkin finite element method with very fine time step and grid size [12]. One can clearly see that the simulated results are identical to the analytical solutions.

7. Conclusions

Many environmental and ecological studies have analyzed overland flow by use of the approximation of kinematic wave theory due to its simplicity and satisfactory accuracy compared to the Saint-Venant hydrodynamic equations. A numerical model is a practical approach for the kinematic overland flow computations in most realistic problems. Some degree of numerical diffusion and oscillation is induced by the finite difference method and the finite element method which are popular numerical schemes used for the overland flow simulations. In this study, the specified-time-interval characteristics method integrated with the cubic-spline interpolation technique (CSMOC scheme) is applied to one-dimensional and two-dimensional kinematic overland flow computations. The characteristic trajectory is allowed to intersect on the space line and time line. The corresponding values at the foot of the trajectory can be approximated in terms of the neighboring grid points. The effects of different endpoint constraints, including the natural constraint, the quadratic constraint, the not-a-knot constraint, the first derivative constraint, and the second derivative constraint, on use of cubic-spline interpolation technique are examined. The results show that as far as accuracy and simplicity are concerned, the not-a-knot constraint could be a better choice. The examination of two one-dimensional hypothetical examples shows that the CSMOC scheme is competitively accurate with the well-known Preissmann scheme for the kinematic wave modeling of overland flow. The numerical dissipation and numerical oscillation induced by the Preissmann scheme will not appear

in the CSMOC scheme. In addition, with the application of the fractional-step method, the CSMOC scheme can accurately simulate the two-dimensional kinematic overland flow.

Appendix A. The time line cubic-spline interpolation

If the characteristics curve intersects the time line at boundaries, the cubic-spline interpolation can be applied to the time line to approximate h_l as follows:

$$h_l = E^{n-\hat{m}_l-1}[(1-\zeta)\Delta t]^3 + F^{n-\hat{m}_l-1}[(1-\zeta)\Delta t]^2 + G^{n-\hat{m}_l-1}[(1-\zeta)\Delta t] + H^{n-\hat{m}_l-1} \tag{A.1}$$

with

$$\zeta = \frac{(i-1)\Delta x}{(h)_{pl}\Delta t} - \hat{m}_l \tag{A.2}$$

where $\hat{m}_l = \mathrm{INT}\lfloor (i-1)\Delta x/(h)_{pl}\Delta t \rfloor$. The coefficients E^k, F^k, G^k, and H^k shown in Eq. (A.1) can be expressed as

$$E^k = \frac{R^{k+1} - R^k}{6\Delta t} \tag{A.3}$$

$$F^k = \frac{R^k}{2} \tag{A.4}$$

$$G^k = \frac{h_1^{k+1} - h_1^k}{\Delta t} - \frac{2\Delta t R^k + \Delta t R^{k+1}}{6} \tag{A.5}$$

$$H^k = h_1^k \tag{A.6}$$

where $k = 1, 2, \ldots, NT-1$ in which 1 denotes initial time level and NT represents total time level shown in Fig. 3. R^k, second derivatives for h with respect to temporal coordinate at upstream boundary (grid point $i = 1$) and time level k, could be expressed as following relation

$$R^{k-1} + 2R^k + R^{k+1} = \frac{6}{\Delta t^2}\left(\phi_1^{k-1} - 2\phi_1^k + \phi_1^{k+1}\right) \quad k = 2, 3, \ldots, NT-1 \tag{A.7}$$

According to the natural cubic-spline interpolation, two additional constraints on second derivative with respect to time at initial time level and total time level, i.e. R^1 and R^{NT}, could be represented as

$$R^1 = 0 \tag{A.8}$$

$$R^{NT} = 0 \tag{A.9}$$

References

[1] Ahmad Z, Kothyari UC. Time-line cubic spline interpolation scheme for solution of advection equation. Comput Fluids 2001;30:737–52.

[2] Brakensiek DL. Kinematic flood routing. Trans ASAE 1967;10(3):340–3.

[3] DeBoor C. A practical guide to spline. New York: Springer-Verlag; 1978.

[4] de Lima JLMP, Singh VP. The influence of the pattern of moving rainstorms on overland flow. Adv Water Resour 2002;25:817–28.

[5] Gerald CF, Wheatley PO. Applied numerical analysis. New York: Addison-Wesley; 1994.

[6] Govindaraju RS, Jones SE, Kavvas ML. On the diffusion wave model for overland flow. I: Solution for steep slopes. Water Resour Res 1988;24(5):734–44.

[7] Govindaraju RS, Kavvas ML, Jones SE. Approximate analytical solutions for overland flows. Water Resour Res 1990;26(11): 2903–12.

[8] Heatwole CD, Shanholtz VO, Ross BB. Finite element model to describe overland flow on an infiltrating watershed. Trans ASAE 1982;24(1):630–7.

[9] Hjelmfelt Jr AT. Overland flow from time-distribution rainfall. J Hydraul Div—ASCE 1981;107(2):227–38.

[10] Holden AP, Stephenson D. Finite difference formulations of kinematic equations. J Hydraul Eng 1995;121(5): 423–6.

[11] Jaber FH, Mohtar RH. Stability and accuracy of finite element schemes for the one-dimensional kinematic wave solution. Adv Water Resour 2002;25:427–38.

[12] Jaber FH, Mohtar RH. Stability and accuracy of two-dimensional kinematic wave overland flow modeling. Adv Water Resour 2003;26:1189–98.

[13] Karpik SR, Crockett SR. Semi-Lagrangian algorithm for two-dimensional advection–diffusion equation on curvilinear coordinate meshes. J Hydraul Eng 1997;123(5):389–401.

[14] Knott GD. Interpolating cubic splines. New York: Birkhauser Boston; 1999.

[15] Kvasov BI. Shape-preserving spline approximation. Singapore: Scientific Publishing; 2000.

[16] Lai C. Comprehensive method of characteristics models for flow simulation. J Hydraul Eng 1989;114:1074–97.

[17] Lai C. Modeling alluvial-channel flow by multimode characteristics method. J Eng Mech 1991;117:32–53.

[18] Lai C. Multicomponent-flow analysis by multimode method of characteristics. J Hydraul Eng 1894;120:378–95.

[19] Parlange JY, Rose CW, Sander G. Kinematic flow approximation of runoff on a plane: an exact analytical solution. J Hydrol 1981;52:171–6.

[20] Singh VP. Kinematic wave modeling in water resource resources: surface-water hydrology. New York: Wiley; 1996.

[21] Sharda VN, Singh SR. A finite element model for simulating runoff and soil erosion form mechanically treated agricultural lands. 1. Governing equations and solutions. Water Resour Res 1994;30(7):2287–98.

[22] Schohl GA, Holly Jr FM. Cubic-spline interpolation in Lagrangian advection computation. J Hydraul Eng 1991;117 (2):248–53.

[23] Stefanovic DL, Stefan HG. Accurate two-dimensional simulation of advective–diffusive–reactive transport. J Hydraul Eng 2001; 127(9):728–37.

[24] Thomas LH. Elliptic problems in linear difference equations over a network. Columbia, NY: Waston Scientific Computing Laboratory; 1949.

[25] Tsai TL, Yang JC, Huang LH. An accurate integral-based scheme for advection–diffusion equation. Commu Numer Meth Eng 2001;17:701–13.

[26] Tsai TL, Yang JC, Huang LH. Hybrid finite-difference scheme for solving the dispersion equation. J Hydraul Eng 2002;128(1): 78–86.

[27] Tsai TL, Yang JC, Huang LH. Characteristics method with cubic-spline interpolation for solving the advection–diffusion equation. J Hydraul Eng 2004;130(7):580–5.
[28] Tsai TL, Chiang SW, Yang JC. Characteristics method with cubic-spline interpolation for open channel flow computation. Int J Numer Meth Fluids 2004;46:663–83.
[29] Weinmann PE, Laurenson EM. Approximation flood routing methods: a review. J Hydraul Div: ASCE 1979;105(12): 1521–36.
[30] Yaneko NN. The method of fractional steps: the solution of problems of mathematical physics in several variables. New York: Springer; 1971.